Lawrence Berkeley National Laboratory

Title

Three-Dimensional Surface Downwelling Longwave Radiation Clear-Sky Effects in the Upper Colorado River Basin

Permalink

https://escholarship.org/uc/item/7zj164m2

Journal

Geophysical Research Letters, 49(4)

ISSN

0094-8276

Authors

Feldman, DR
Worden, M
Falco, N
et al.

Publication Date

2022-02-28

DOI

10.1029/2021gl094605

Peer reviewed

RESEARCH LETTER

Key Points:

- In mountains, warmer, snow-free surfaces emit more longwave energy that heat up colder, snow-covered surfaces
- ECOSTRESS data show that this 3-D effect is spatially variable, accounting for ~22% of surface longwave flux in the Upper Colorado River
- Most weather and climate models do not include this 3-D effect and therefore underestimate surface longwave energy in complex terrain

Supporting Information:

Supporting Information may be found in the online version of this article.

Correspondence to:

D. R. Feldman,
drfeldman@lbl.gov

Author Contributions:

Conceptualization: D. R. Feldman
Data curation: D. R. Feldman, M. Worden
Formal analysis: D. R. Feldman, M. Worden, N. Falco, J. Chen, B. Dafflon, H. Wainwright
Funding acquisition: H. Wainwright
Investigation: D. R. Feldman, M. Worden, N. Falco, P. J. Dennedy-Frank, J. Chen, B. Dafflon, H. Wainwright
Methodology: D. R. Feldman, N. Falco, P. J. Dennedy-Frank, J. Chen, B. Dafflon, H. Wainwright

Three-Dimensional Surface Downwelling Longwave Radiation Clear-Sky Effects in the Upper Colorado River Basin

D. R. Feldman[1] ![ORCID], **M. Worden**[1,2], **N. Falco**[1] ![ORCID], **P. J. Dennedy-Frank**[1] ![ORCID], **J. Chen**[1] ![ORCID], **B. Dafflon**[1] ![ORCID], and **H. Wainwright**[1]

[1]Lawrence Berkeley National Laboratory, Berkeley, CA, USA, [2]Department of Earth System Science, Stanford University, Stanford, CA, USA

Abstract In complex terrain, non-parallel surfaces receive emitted radiation from adjacent surfaces. Qualitatively, where surface skin temperatures and lower tropospheric temperature and humidity are not uniform, the downwelling longwave radiation (DLR) will be determined not just by radiation from the atmosphere above a given location, but also by adjacent surface temperatures. We quantify this three-dimensional longwave radiative effect over the Upper Colorado River Basin in clear-sky conditions by calculating surface DLR with observed land-surface temperatures from ECOSTRESS. We find that this effect is due to terrain-subtended sky-view and represents ~22% of the surface longwave flux, rising to ~28% and ~24% in the East and Southeast of the Basin, respectively, and can be >50% in extreme cases. The common omission of this effect in atmospheric radiation models leads to an underestimation of DLR in complex terrain, especially at higher elevations, which has significant implications for mountainous ecohydrology simulations.

Plain Language Summary In the mountains, snowmelt is driven primarily by more sunlight and secondarily by warmer temperatures, but as areas become snow-free, they will warm much faster during the day than snow-covered ones will. The snow-free surfaces will radiate onto the snow-covered surfaces, warming them and melting them even faster. While this effect is well understood in principle, its size and where it is occurring are not, since they depend both on terrain and on what surface temperatures actually are. We use a thermal camera mounted on the International Space Station called ECOSTRESS to show how large this 3-dimensional effect is in the Upper Colorado River from which nearly all of that river's water is derived. We show that the effect is concentrated in the Upper Gunnison River and that most hydrological models do not include it. However, fixing that omission will tend to exacerbate hydrological model biases in predicting snowmelt, suggesting that more snowmelt modeling work is needed.

1. Introduction

Approximately half of the world relies on water resources derived from mountains (Huss et al., 2017). Unfortunately, these resources have been dwindling, and there is significant concern that they will be even more threatened in the future (Sturm et al., 2017), with changes in the phase and amount of precipitation in high-altitude complex terrain. The Colorado River Watershed is a prime example where dwindling snowpack (Mote et al., 2018) and diminished flows (Milly & Dunne, 2020) compound to impact water resources on which millions of people rely (James et al., 2014).

High-altitude complex terrain is particularly problematic for modeling and observations, largely driven by first-order spatiotemporal heterogeneity in the processes that impact hydrology. Radiation is one such process of primary importance for mountainous hydrology (Brubaker et al., 1996; Kustas et al., 1994; Mizukami et al., 2014). Longwave radiation has long been recognized as a key driver in the modeling of snowmelt (Brutsaert, 1975; Marks & Dozier, 1979), impacting the timing and availability of water resources from this source (Rhoades et al., 2018). In addition, radiation, slopes, and aspects are key controls on ecosystem processes and drought vulnerability (e.g., Wainwright et al., 2020).

Ohmura (2001) found both from a theoretical and phenomenological perspective that downwelling longwave radiation (DLR) is the main energy source for snowmelt. This finding was confirmed both by Hock (2003) and M. Zhu et al. (2017), where those works highlight the myriad dynamic and thermodynamic processes that govern surface temperature in complex terrain.

DLR at a given location is a function of total hemispheric emission, and is therefore determined by the longwave emission of the atmosphere and the longwave emission, which itself is determined by skin temperature and emissivity, from terrain that subtends the location's sky-view. The importance of terrain effects on DLR has been confirmed by limited observations that noted emission temperatures of rocks in snow-covered environments can be more than 20 K above freezing (Olyphant, 1986; Sicart et al., 2006). Recently, a number of publications have recognized the importance of topography for longwave radiation in complex terrain (Yan et al., 2016, 2020), and found that topographic radiative effects may impact precipitation and snowmelt and need to be included in models to avoid biases (Gu et al., 2020; Lee et al., 2015).

Radiometrically accurate modeling in mountainous complex terrain must recognize the geometric effects from this terrain, though many radiation solvers use plane-parallel formulations and incur errors. The importance of 3-D shortwave effects has been shown to have strong impacts on the location, timing, and amount of snow-melt (Palazzi et al., 2019), and a parameterization, based on adjustments to a plane-parallel calculation built from Monte Carlo codes, have been developed (Lee et al., 2015) and implemented in the Community Land Model (CLM; Lee et al., 2019) and the Energy Exascale Earth System Model (E^3SM; Hao et al., 2021). Still, the use of parameterizations of 3-D longwave radiative effects is exceedingly rare, even though these effects can be instantaneously larger than 100 W/m^2 and represent the dominant source of uncertainty in forcing of the snowpack (Raleigh et al., 2015).

Plüss and Ohmura (1997) discussed terrain effects on DLR extensively and proposed a simple parameterization based on local air and surface temperature that is predicated on a fixed amount of snow-cover at a given location. However, there has been insufficient spatiotemporal data to quantify the qualitatively understood error incurred by omitting terrain effects from estimates of DLR in complex terrain. Thermal imagery from satellite instruments characterizes spatial variability in the thermal environment but imagery from, for example, MODIS or GOES, is of coarse resolution (~1 and ~2 km, respectively) relative to the relevant terrain effects (see Figure 2 and also Lipton, 1992; Lipton & Ward, 1997). While instruments such as Landsat and ASTER provide thermal imagery at much higher spatial resolution (~100 m for Landsat 8 and ~90 m for ASTER), those measurements are made on a sun-synchronous platform and are therefore unable to measure across a diurnal cycle to capture the temporal dynamics of differential land-surface heating in mountains (Hock, 1999, 2005; Hock et al., 2005; Singh & Kumar, 1996).

The novelty of the research presented here is that it is based on calculations informed by high-resolution thermal imagery from the ECOsystem Spaceborne Thermal Radiometer Experiment on Space Station (ECOSTRESS) instrument across an entire mountain basin: the Upper Colorado River Basin (UCRB). ECOSTRESS produces unique space-based thermal imagery, with 70-m resolution at an inclined orbit aboard the International Space Station, thereby acquiring snapshots of the surface thermal environments in high-altitude complex terrain at a wide range of local solar hours (Fisher et al., 2020). ECOSTRESS surface skin temperature measurements are derived from mid-infrared radiometric observations in 3 micro-windows spanning wavelengths between 8 and 12 μm. The orbit of the International Space Station precesses across the local diurnal cycle, which enables high spatial resolution and measurements at different local solar hours. While ECOSTRESS does not continuously sample a given area like geostationary platforms can, or sample regularly, such as with the 16-day repeat time of sun-synchronous platforms, it does collect thermal imagery across a range of local times unlike sun-synchronous platforms and does so at much higher spatial resolution than GOES-16 observations (70 m vs. 2 km).

In this paper, we explore the importance of terrain for DLR in the UCRB using the novel, intermittent, potentially gap-filling data introduced from ECOSTRESS. We present an initial analysis of 2 years of ECOSTRESS observations to characterize the importance of terrain effects to DLR calculations and discuss the lessons that can be learned from these observations for model parameterization development. We show the value of resolution and spatial variability for characterizing DLR, that it contributes to snowmelt especially in specific locations of the UCRB, and that terrain effects should be included in hydrological models to avoid low-biases in the surface energy budget.

2. Methods

The first part of the analysis presented here focuses on the 300 km^2 near Crested Butte, Colorado, since it is heavily studied and provides synergistic research opportunities with field work and campaigns such as the Watershed Function Scientific Focus Area and the Surface Atmosphere Integrated Field Laboratory (SAIL) (Feldman et al., 2021; Hubbard et al., 2018). The latter part of the analysis presented here looks at the UCRB, covering 285,000 km^2 of the Southwestern United States including portions of Wyoming, Utah, Colorado, New Mexico, and Arizona. We analyze this area because nearly all of the water resources of the much larger (640,000 km^2) Colorado River Watershed are derived from this watershed (Tillman, 2015). The UCRB contributes to water for 40 million people, enables ~53 GW of electric power generation capacity, supports ~\$1.3 Trillion of economic activity annually, and provides ~15 million jobs (James et al., 2014), while being the most hydrologically significant watershed in North America (Messerli et al., 2004).

We use the ECOSTRESS land surface temperature and emissivity (LSTE) Product at 70-m resolution, which includes retrievals of land surface temperature (LST) under clear-sky conditions. The instrument collects data at a given location at irregular intervals and at varying times of day, since it is manifested on the International Space Station (ISS) and collects data according to the ISS orbit. Given the difficulty in determining LST from ECOSTRESS in the presence of clouds, we only use LST data for which the ECOSTRESS reports cloud-free conditions with quality-assurance flags reporting good quality L1B data and <1 K LST accuracy. The approach used for determining whether pixels are cloud-contaminated uses thermal tests developed directly from the MODIS and VIIRS cloud mask algorithms (Hulley, 2016). In addition, we use 30-m terrain data from the Global Digital Elevation Model Version 3 from the Advanced Spaceborne Thermal Emission and Reflection Radiometer (ASTER; Abrams et al., 2020) for elevation, slope, and aspect calculations area-averaged to 70-m. Finally, we use snow depth retrievals from the Airborne Snow Observatory (ASO) surveys (Painter et al., 2016) collected in 30–31 March, 2018 and 24 May 2018.

We use the approach of Plüss and Ohmura (1997), which provides a set of formulas for calculating terrain effects on DLR: the DLR at a given location is the result of integrated radiance contributions from sky and terrain, as shown in Equations 1a–1f.

$$\text{DLR} = L_a^\downarrow + L_s^\downarrow \tag{1a}$$

$$L_a^\downarrow = \int_0^{2\pi} \int_{H(\varphi)}^{\pi/2} I_a(\theta, \varphi) \cos i \cos H \, d H \, d\varphi \tag{1b}$$

$$\cos i = \sin\beta \cos\varphi \cos H + \cos\beta \, \sin H \tag{1c}$$

$$L_s^\downarrow = \sum_j^N \sum_k^M \left(L_B + aT_a + bT_s^{j,k} \right) \Omega^{j,k} \tag{1d}$$

$$\Omega^{j,k} \cong 2\pi \left(1 - \cos\frac{\gamma^{j,k}}{2} \right) \tag{1e}$$

$$I_a(\theta, \varphi) = 0.642 \left(\frac{e_a}{T_a} \right)^{\frac{1}{7}} \left(\sigma T_a^4 \right) \tag{1f}$$

where $L_a^\downarrow$ is the portion of the DLR from the atmosphere (sky) and $L_s^\downarrow$ is the portion of the DLR from surface (terrain). The sky radiance I_a is formally a function of zenith angle θ and azimuth angle φ and, practically speaking, it can be adequately represented as a function of near-surface humidity e_a and near-surface air temperature T_a as shown in Equation 1f from Brutsaert (1975). In Equation 1b, the lower interval bound for zenith integration over the sky is set by the elevation angle H, which varies azimuthally. The angle i between the vector vertical to the surface and the vector of interest is given in Equation 1c as a function of inclined surface inclination angle β. The terrain irradiance is given in Equation 1d where the summation terms are based on the parameterization of terrain radiance where L_B is the emitted radiance of a 0°C blackbody, and a and b are spatially invariant constants in a parameterization, as given in Plüss and Ohmura (1997). The summation index j represents discretization of azimuth angle for a given radius and the summation index k represents the discretization of radius. Each summation

term in Equation 1d represents the contribution of radiance to the total irradiance by including the discrete solid angles $\Omega^{j,k}$ subtended by terrain elements at a range of radii and azimuth angles from the surface of interest. The summation of azimuth angle is discretized into N intervals over 2π radians with M radius increments, where radius increments practically extend 2 km from the surface of interest (and was verified with heuristic tests in the Supporting Information S1) (Lipton, 1992; Lipton & Ward, 1997). In Equation 1e, we approximate the solid angle subtended by a terrain element at a given radius and azimuth by determining the unobstructed viewing angle $\gamma^{j,k}$ from the surface of interest to the terrain element j, k and using the formula for the solid angle of a cone, following the sky-view calculation in complex terrain of Zakšek et al. (2011). This formulation neglects thermal scattering and simplifies atmospheric emission and treats surface emissivity as a scalar term, but the use of the Brutsaert (1975) formulation and the omission of thermal scattering has been found to incur mean bias errors of less than 2.5 W/m^2 relative to field observations (Howard & Stull, 2013; M. Zhu et al., 2017) and has been shown to be reasonable for clear-sky conditions in complex terrain (Bennett et al., 1960; Flerchinger et al., 2009; Unsworth & Monteith, 1975), to which we limit the analysis presented here.

We use the formulae in Equations 1a–1f to develop instantaneous maps of DLR based on ECOSTRESS surface temperature observations in Equation 1c. Surface air temperature (SAT) and surface humidity are required for Equation 1f, and we set SAT to 3°C less than LST observations and humidity to 50% of saturation vapor pressure. We test the impact of systematic biases in SAT and surface humidity with sensitivity tests based on ECMWF reanalysis fields in the Supporting Information S1 and we find that error in SAT and surface humidity produces a second-order effect on DLR, at less than 10 W/m^2 and find that DLR is sensitive to LST to first order and SAT and surface humidity to second-order.

We also calculate the fraction of DLR from terrain contributions by comparing the results from Equations 1d and 1b, including across the entire UCRB. We recognize that an analysis of the collective impacts of terrain on DLR across the diurnal cycle is an important consideration. We therefore develop diurnally averaged contributions of the terrain to DLR simply by averaging the instantaneous snapshots of observationally derived DLR from Equation 1 and rationale and limitations of that approach below.

Finally, we briefly look into the forcing that terrain effects exert on the snowpack. We overlay the longwave clear-sky DLR with the change in snow depth measured by the Airborne Snow Observatory (ASO) measured from the end-of-winter peak to early May for a range of slope and aspects.

3. Results

The relationship between the LST measurements and DLR is shown in Figure 1, which presents instantaneous LST measurements from ECOSTRESS and our corresponding calculations of DLR using Equations 1a–1f. In spite of data gaps from clouds, these plots predictably show generally increasing surface temperatures with increasing solar elevation angle for several snapshots in June 2020, though we recognize that surface temperature is strongly influenced by local meteorological conditions, and that these snapshots may be associated with different weather systems. At the same time, though, the DLR calculations in Figure 1 corresponding to those LST measurements, while having more gaps due to clouds causing outages in DLR calculations of adjacent pixels, do exaggerate gradients in surface temperature and produce persistent "hot-spots" (indicated with blue arrows). These "hot-spots," such as the northwestern and western sides of the domain are shown in Figure 1, and are concentrated where the fraction of the sky visible from a given location (its sky-view) is most subtended by terrain with surrounding warm surfaces.

In Figure 2, we show the importance of spatial resolution in resolving these 3-dimensional longwave radiative effects at the surface. The panels of the figure show calculations following Equations 1a–1f of diurnally averaged DLR at 70-m resolution and successive calculations where both surface temperature and terrain were area-averaged to 500-m, 1 km, and 2 km resolution, with the latter resolution corresponding to the resolution of geostationary observations. These illustrate that a significant amount of spatial information is obscured at 500 m resolution, and then generally corrupted at 1 and 2 km resolution.

Domain-wide bias and RMSE statistics for different resolutions are presented in Figures 2e and 2f, respectively. These plots show that under-resolving complex terrain can lead to remarkably large domain-average bias and RMSE values: DLR exhibits a low bias by ~30 W/m^2 and an RMSE of ~45 W/m^2 for 2 km resolution versus
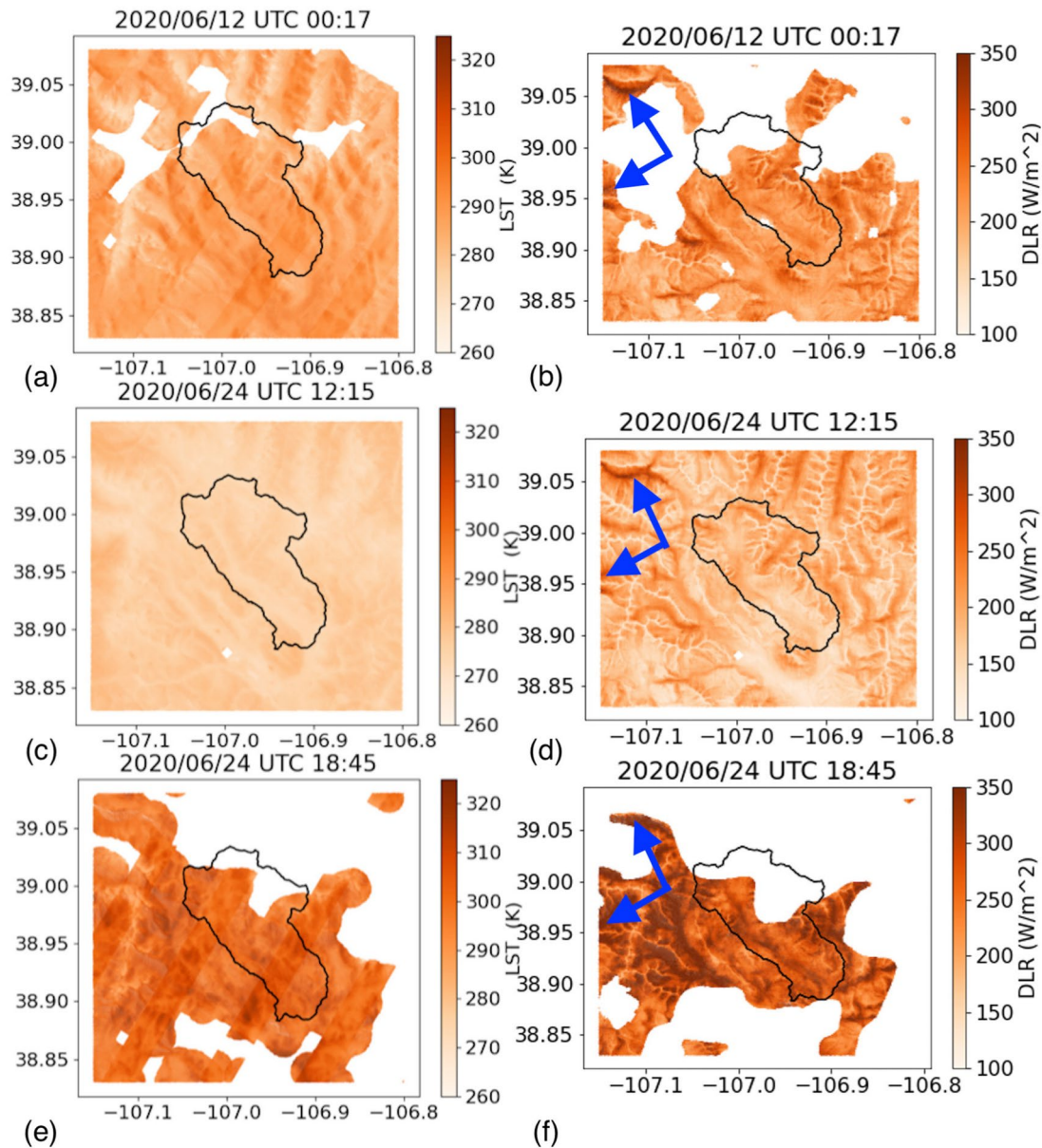
Figure 1. (a) Instantaneous ECOsystem Spaceborne Thermal Radiometer Experiment on Space Station (ECOSTRESS) land surface temperature (LST) observation over ERW (outlined in black) on 12 June 2020 at UTC 00:17 (18:17 Mountain Standard Time [MST]). (b) Instantaneous calculation of downwelling longwave radiation (DLR) over ERW on 12 June 2020 at UTC 00:17, based on ECOSTRESS LST observation. (c and d) Same as (a and b) but on 24 June 2020 at UTC 12:15 (06:15 MST). (e and f) Same as (a and b) but on 24 June 2020 at UTC 18:45 (12:45 MST). Blue arrows in (b, d, and f) highlight "hot-spots" of persistently high DLR from terrain.

70 m resolution. The heuristic plots in Figures 2e and 2f address whether 70 m resolution is, itself, sufficient to produce unbiased and low RMSE estimates of DLR. From the shape of the RMSE heuristic curve, which grows quasi-logarithmically with resolution, there may not be additional information from including higher-resolution information. The bias heuristic is strictly positively signed, implies both that the exclusion of terrain-effects systematically underestimates DLR and that LST observations collected both by GOES and polar-orbiting instruments like MODIS and VIIRS at 2 and 1 km resolution, respectively, underestimate DLR by under-resolving terrain effects.

Next, we show a comparison of shortwave and longwave terrain effects for illustrative purposes in Figure 3. This figure shows changes in ASO-derived snow-depth change during spring melt from 30 March 2018 to 24 May
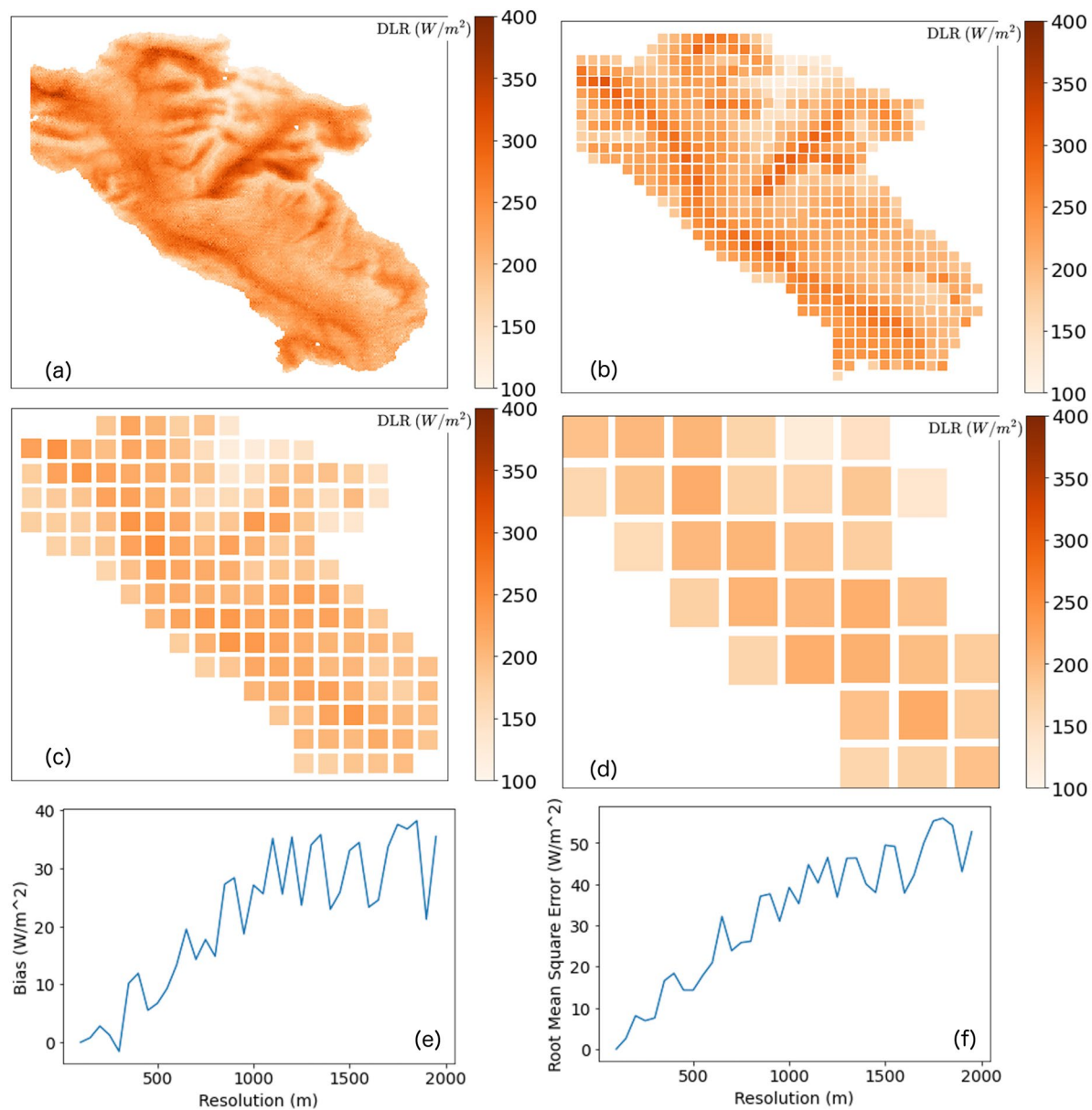
Figure 2. (a) Diurnally averaged downwelling longwave radiation (DLR) (W/m²) calculated over ERW (outlined in black) in the Upper Colorado River Basin at 70 m resolution from June 2020. (b) Same as (a) but recalculated with surface temperatures and elevation area-averaged to 500 m resolution. (c) Same as (b) but with resampling to 1 km resolution. (d) Same as (d) but with resampling to 2 km resolution. (e) ERW-averaged DLR bias (abscissa value minus 70 m value) as a function of resolution. (f) Same as (e) but showing ERW-averaged RMSE as a function of resolution.

2018 with overlays of longwave radiation contours. The radiation contours are calculated from ECOSTRESS observations available in the spring of 2020. We recognize that these are not temporally collocated, but since we do not have ASO surveys that measure snowmelt during the period where ECOSTRESS has collected data, we are displaying these results for illustrative purposes. We also note that there is some interannual consistency, scaled by the amount of precipitation received in a given year, to the spatial patterns of snow deposition and melt in this area (Raleigh et al., 2019). The callout boxes in Figure 3 show areas with enhanced longwave radiation and show the distributions of terrain aspect, slope, and sky-view. In the callouts, snow-melt loosely follows gradients in DLR, but variation in slope, aspect, and sky-view point to multiple factors influencing the surface energy balance, not just in the longwave but also in the shortwave. The Supporting Information S1 explores these spatial relationships in more detail.
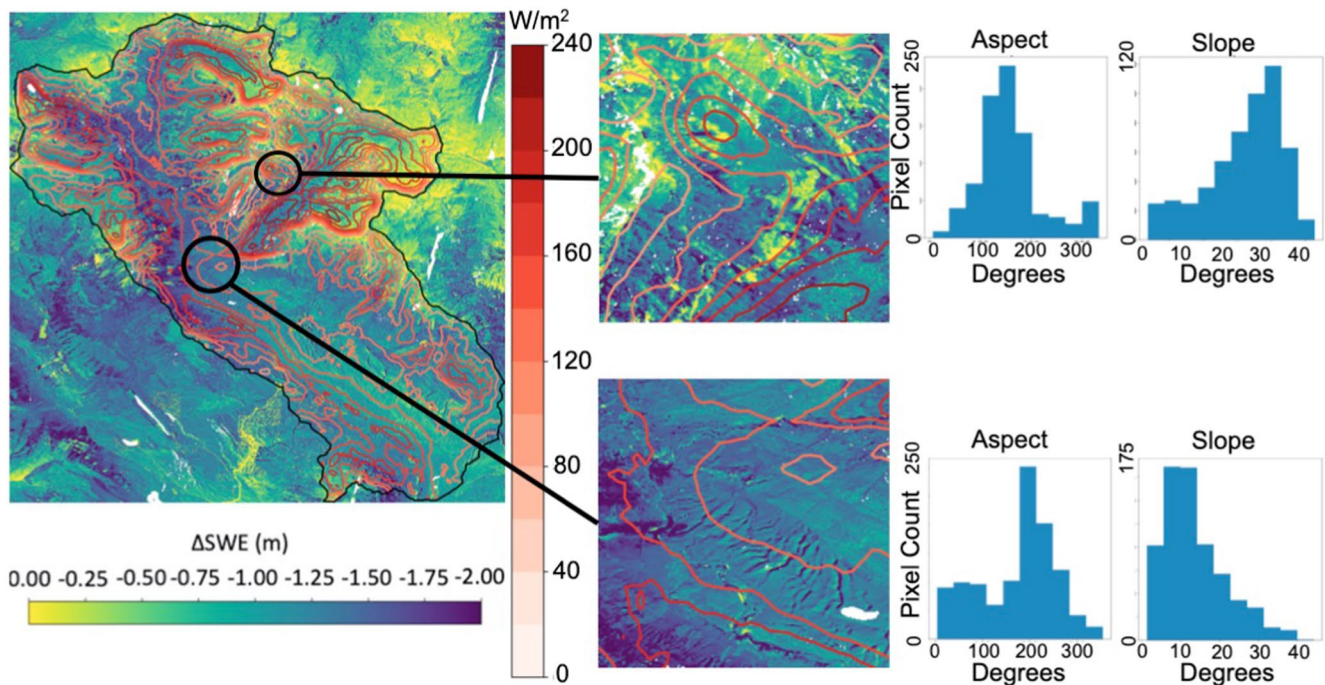
Figure 3. Upper left panel shows contours of springtime clear-sky downwelling longwave radiation at the surface over the ERW. Underlying color contours show change (May 2018–April 2018) in SWE measured by ASO. Three callout regions of the ERW along with distributions of their terrain slope, aspect, and sky-view are also shown.

Figure 4 expands the analysis across the UCRB to quantify the percentage of DLR from terrain effects in $2° \times 2°$ sub-regions for all observations from ECOSTRESS between April and June 2020. The histograms show the fractional contribution of the terrain to DLR from instantaneous ECOSTRESS LST observations as a function of elevation in each subset. The first finding from this UCRB-wide analysis is that there is a surprising amount of variability in the histograms for different sub-regions of the UCRB. Some sub-regions of the UCRB, for example, the east and southeast exhibit the largest terrain effects, while the northern and southwestern sub-regions exhibit the smallest terrain effects. The spatial variability is driven by sky-view factor variability in each sub-region (see Supporting Information S1). In the east and southeast, 24.3% and 27.8% of DLR is contributed by terrain across most elevations, respectively, while terrain effects on DLR in the north are 22.8%, and the southwest are 17.5%. Together, the average terrain contribution to DLR is 21.6% across the UCRB.

In Figure 5, the effects of neglecting terrain effects on DLR are shown across the UCRB. Again depending on sky-view, terrain effects can induce very large biases, and some of these biases are concentrated in narrow elevation ranges for different sub-regions, especially in the northern sub-region of the UCRB. These findings shows that shorter-term biases in DLR from neglecting terrain effects can be up to 100 W/m^2 and that those biases extend across the UCRB.

4. Discussion

Together, these results point to the role of fine-scale terrain in influencing the surface radiative energy budget, and that the well-known terrain effects on shortwave radiation need to be evaluated alongside terrain effects on longwave radiation. Specifically, from ECOSTRESS LST observations, we find that terrain effects exaggerate gradients in LST to produce "hot-spots" in DLR over the UCRB that persist across diurnal to synoptic variability in LST. We find that calculations of the thermal energy environment that do not explicitly account for terrain effects will be low-biased and have very large RMSEs if these effects are not resolved below 500 m. We also show that significant longwave and shortwave terrain effects are not necessarily collocated. UCRB-wide analysis reveals that longwave terrain effects are spatially concentrated in the East and Southeast of the UCRB due to diminished sky-view in those areas.
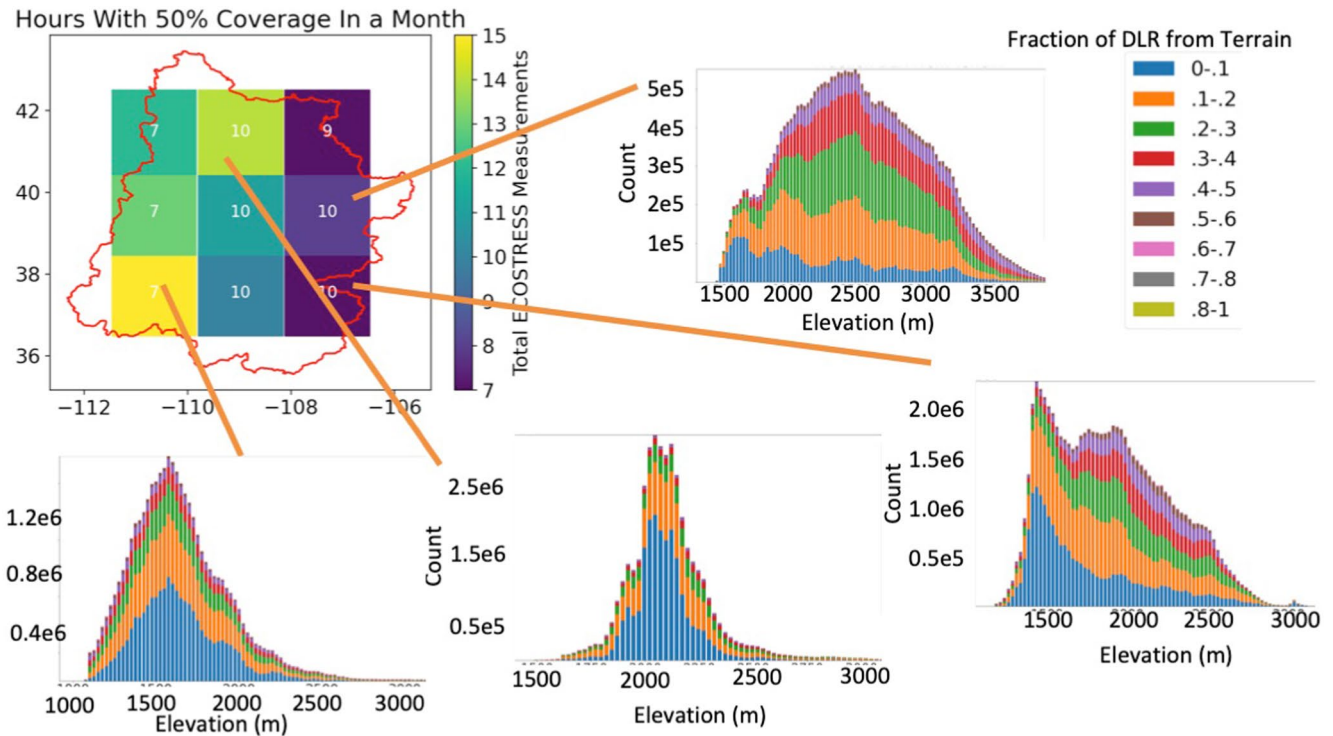
Figure 4. Elevation-resolved histogram of the fraction of downwelling longwave radiation from terrain, with calculations derived from ECOsystem Spaceborne Thermal Radiometer Experiment on Space Station (ECOSTRESS) in $2° \times 2°$ sub-regions across the Upper Colorado River Basin (UCRB) between April and June 2020. The center depicts the entire UCRB and its sub-regions with a number in each sub-region indicating the maximum local solar hour time between ECOSTRESS observations used to develop diurnal cycle averages, while the color of the sub-region indicates how many ECOSTRESS observations are acquired for that sub-region.
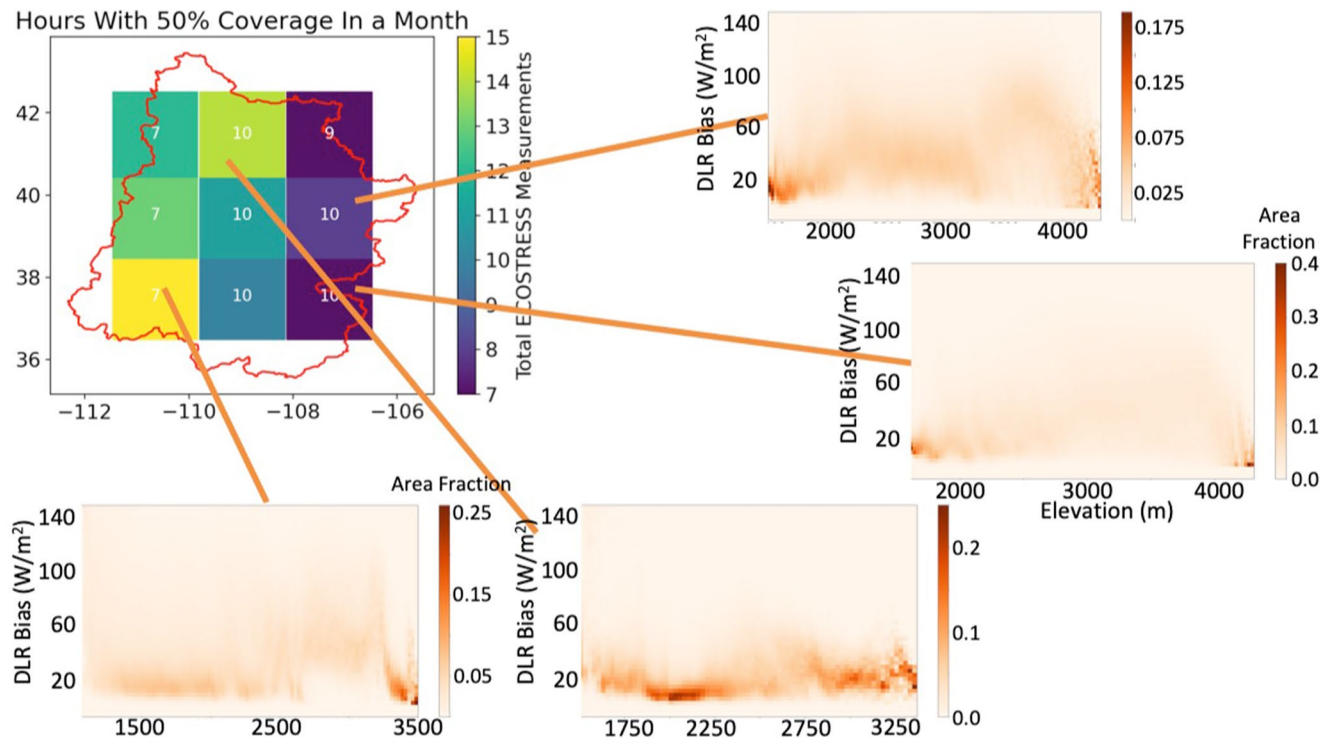

Figure 5. Same as Figure 4 except showing two-dimensional elevation-resolved histograms of DLR bias from neglecting topographic effects.

However, there are several caveats to these results. First, the approach we took to determine DLR used reanalysis values for surface air temperature and humidity, which could incur error up to 10 W/m² (see Supporting Information S1).

Second, for diurnally averaged estimates, we would prefer to use LST observations from ECOSTRESS in an assimilation framework, but do not have a competent model for LST diurnal cycle in complex terrain at the resolution of ECOSTRESS.

Third, LST retrievals from ECOSTRESS, while subjected to validation activities (Hulley et al., 2021), may contain biases in complex terrain since terrain elements need to be incorporated in such retrievals. Otherwise, they can be biased high by as much as 1 K in algorithms that do not include these effects (Lipton, 1992; Lipton & Ward, 1997; X. Zhu et al., 2020) and ECOSTRESS georegistration accuracy in complex terrain (Smyth, 2018) can induce uncertainty in the analysis.

Fourth, for this analysis, we only considered clear-sky conditions. LW terrain effects are strongest in the clear-sky due their ability to produce to higher surface temperatures, so these results provide a likely upper-bound on 3-D LW radiative effects in complex terrain. Finally, we only focused on a limited time-period at the end of spring melt where LST over snow-covered surfaces remains near the freezing point while LST over snow-free surfaces can vary by more than 30°K (see Supporting Information S1). We expect terrain effects to be smaller than what is presented here in the cold season, though they could be comparable in the warm season.

Despite these caveats, there are implications for the representation of atmospheric and surface radiation in complex terrain from these findings. From these findings, it is reasonable to recommend that longwave terrain effects be included in atmospheric and surface models. Models across a range of complexities, from atmospheric process models like the Weather Research and Forecasting (WRF) model to Earth System Models generally do not include these effects. The persistence of exaggerated effects of terrain on DLR across meteorological conditions and the strong dependence of these effects on topography suggest that the contributions of terrain to DLR would be amenable to a straightforward sub-grid parameterization based on DEM, surface temperature, and fractional snow coverage. Given our finding that a low-bias in DLR is incurred in surface energy budgets of models of high-altitude complex terrain from the omission of three-dimensional longwave effects, the inclusion of these effects in models will impact their fidelity with regards to snowpack and snow processes (Essery et al., 2009, 2013; Feng et al., 2008), which have been identified as a major area of weakness for land surface models (Dirmeyer et al., 2006). The inclusion of these effects will also exacerbate the common issue in reanalyses and regional and global climate models wherein they produce erratic year-to-year melt rates relative to observationally constrained snow products (Rhoades et al., 2018). It will do so by tending to increase DLR and produce greater forcing on the snowpack and increased snowmelt.

Data Availability Statement

ECOSTRESS data are freely available and can be downloaded from https://ecostress.jpl.nasa.gov/data. The ASTER GDEM is freely available to download from https://asterweb.jpl.nasa.gov/gdem.asp. GOES-16 data are freely available to download from https://noaa-goes16.s3.amazonaws.com/index.html. ASO snow depth data are freely available to download from https://nsidc.org/data/ASO_50M_SD/versions/1.

References

Abrams, M., Crippen, R., & Fujisada, H. (2020). ASTER Global Digital Elevation Model (GDEM) and ASTER Global Water Body Dataset (ASTWBD). *Remote Sensing*, *12*(7), 1156. https://doi.org/10.3390/rs12071156

Bennett, H. E., Bennett, J. M., & Nagel, M. R. (1960). Distribution of infrared radiance over a clear sky. *Journal of the Optical Society of America*, *50*, 100–106. https://doi.org/10.1364/JOSA.50.000100

Brubaker, K. A., Rango, A., & Kustas, W. (1996). Incorporating radiation inputs into the snowmelt runoff model. *Hydrological Processes*, *10*, 1329–1343. https://doi.org/10.1002/(SICI)1099-1085(199610)10:10<1329::AID-HYP464>3.0.CO;2-W

Brutsaert, W. (1975). On a derivable formula for long-wave radiation from clear skies. *Water Resources Research*, *11*(5), 742–744. https://doi.org/10.1029/WR011i005p00742

Dirmeyer, P. A., Gao, X., Zhao, M., Guo, Z., Oki, T., & Hanasaki, N. (2006). GSWP-2: Multimodel analysis and implications for our perception of the land surface. *Bulletin of the American Meteorological Society*, *87*, 1381–1397. https://doi.org/10.1175/BAMS-87-10-1381

Essery, R., Morin, S., Lejeune, T., & Menard, C. (2013). A comparison of 1701 snow models using observations from an alpine site. *Advances in Water Resources*, *55*, 131–148. https://doi.org/10.1016/j.advwatres.2012.07.013

Essery, R., Rutter, N., Pomer oy, J., Baxter, R., Stähli, M., Gustafsson, D., et al. (2009). SNOWMIP2: An evaluation of forest snow process simulations. *Bulletin of the American Meteorological Society*, *90*, 1120–1135. https://doi.org/10.1175/2009BAMS2629.1

Feldman, D. R., Aiken, A., Boos, W., Carroll, R., Chandrasekar, V., Collins, W., et al. (2021). In R. Stafford (Ed.), *Surface atmosphere integrated field laboratory (SAIL) science plan*, ARM user facility. DOE/SC-ARM-21-004.

Feng, X., Sahoo, A., Arsenault, K., Houser, P., Luo, Y., & Troy, T. J. (2008). The impact of snow model complexity at three CLPX sites. *Journal of Hydrometeorology*, *9*, 1464–1481. https://doi.org/10.1175/2008JHM860.1

Fisher, J. B., Lee, B., Purdy, A. J., Halverson, G. H., Dohlen, M. B., Cawse-Nicholson, K., et al. (2020). ECOSTRESS: NASA's next generation mission to measure evapotranspiration from the international space station. *Water Resources Research*, *56*, e2019WR026058. https://doi.org/10.1029/2019WR026058

Flerchinger, G. N., Xaio, W., Marks, D., Sauer, T. J., & Yu, Q. (2009). Comparison of algorithms for incoming atmospheric long-wave radiation. *Water Resources Research*, *45*, W03423. https://doi.org/10.1029/2008WR007394

Gu, C., Huang, A., Wu, Y., Yang, B., Mu, X., Zhang, X., & Cai, S. (2020). Effects of subgrid terrain radiative forcing on the ability of RegCM4. 1 in the simulation of summer precipitation over China. *Journal of Geophysical Research: Atmospheres*, *125*(12), e2019JD032215. https://doi.org/10.1029/2019JD032215

Hao, D., Bisht, G., Gu, Y., Lee, W.-L., Liou, K.-N., & Leung, L. R. (2021). A parameterization of sub-grid topographical effects on solar radiation in the E3SM land model (Version 1.0): Implementation and evaluation over the Tibetan plateau. *Geoscientific Model Development Discussions*, *14*(10), 6273–6289. https://doi.org/10.5194/gmd-2021-55

Hock, R. (1999). A distributed temperature-index ice- and snowmelt model including potential direct solar radiation. *Journal of Glaciology*, *45*(149), 101–111. https://doi.org/10.3189/S0022143000003087

Hock, R. (2003). Temperature index melt modelling in mountain areas. *Journal of Hydrology*, *282*(1–4), 104–115. https://doi.org/10.1016/S0022-1694(03)00257-9

Hock, R. (2005). Glacier melt: A review of processes and their modeling. *Progress in Physical Geography: Earth and Environment*, *29*(3), 362–391. https://doi.org/10.1191/0309133305pp453ra

Hock, R., Jansson, P., & Braun, L. N. (2005). Modelling the response of mountain glacier discharge to climate warming. In U. M. Huber, H. K. M. Bugmann, & M. A. Reasoner (Eds.), *Global change and mountain regions. Advances in global change research* (Vol. 23, pp. 243–252). Springer. https://doi.org/10.1007/1-4020-3508-X_25

Howard, R., & Stull, R. (2013). Modeling the downwelling longwave radiation over a groomed ski run under clear skies. *Journal of Applied Meteorology and Climatology*, *52*(7), 1540–1553. https://doi.org/10.1175/JAMC-D-12-0245.1

Hubbard, S. S., Williams, K. H., Agarwal, D., Banfield, J., Beller, H., Bouskill, N., et al. (2018). The East River, Colorado, Watershed: A mountainous community testbed for improving predictive understanding of multiscale hydrological–biogeochemical dynamics. *Vadose Zone Journal*, *17*, 1–25, 180061. https://doi.org/10.2136/vzj2018.03.0061

Hulley, G. (2016). *ECOSTRESS level-2 cloud detection algorithm theoretical basis document*. Retrieved from https://lpdaac.usgs.gov/documents/296/ECO2_Cloud_ATBD_V1.pdf

Hulley, G., Göttsche, F. M., Rivera, G., Hook, S. J., Freepartner, R. J., Martin, M. A., et al. (2021). Validation and quality assessment of the ECOSTRESS level-2 land surface temperature and emissivity product. *IEEE Transactions on Geoscience and Remote Sensing*, 1–23. https://doi.org/10.1109/TGRS.2021.3079879

Huss, M., Bookhagen, B., Huggel, C., Jacobsen, D., Bradley, R. S., Clague, J. J., et al. (2017). Toward mountains without permanent snow and ice. *Earth's Future*, *5*, 418–435. https://doi.org/10.1002/2016EF000514

James, T., Evans, A., Madly, E., & Kelly, C. (2014). *The economic importance of the Colorado River to the basin region*. Final Report. L. William Seidman Research Institute, Arizona State University. Retrieved from https://businessforwater.org/wp-content/uploads/2016/12/PTF-Final-121814.pdf

Kustas, W. P., Rango, A., & Uijlenhoet, R. (1994). A simple energy budget algorithm for the snowmelt runoff model. *Water Resources Research*, *30*(5), 1515–1527. https://doi.org/10.1029/94WR00152

Lee, W.-L., Gu, Y., Liou, K. N., Leung, L. R., & Hsu, H. H. (2015). A global model simulation for 3-D radiative transfer impact on surface hydrology over the Sierra Nevada and Rocky Mountains. *Atmospheric Chemistry and Physics*, *15*, 5405–5413. https://doi.org/10.5194/acp-15-5405-2015

Lee, W.-L., Liou, K.-N., Wang, C.-c., Gu, Y., Hsu, H.-H., & Li, J.-L. F. (2019). Impact of 3-D radiation-topography interactions on surface temperature and energy budget over the Tibetan Plateau in winter. *Journal of Geophysical Research: Atmospheres*, *124*, 1537–1549. https://doi.org/10.1029/2018JD029592

Lipton, A. E. (1992). Effects of slope and aspect variations on satellite surface temperature retrievals and mesoscale analysis in mountainous terrain. *Journal of Applied Meteorology*, *31*, 255–264. https://doi.org/10.1175/1520-0450(1992)031<0255:EOSAAV>2.0.CO;2

Lipton, A. E., & Ward, J. M. (1997). Satellite-view biases in retrieved surface temperatures in mountain areas. *Remote Sensing of Environment*, *60*, 92–100. https://doi.org/10.1016/S0034-4257(96)00165-4

Marks, D., & Dozier, J. (1979). A clear-sky longwave radiation model for remote alpine areas. *Geophysik und Bioklimatologie, Serie B*, *27*, 159–178. https://doi.org/10.1007/BF02243741

Messerli, B., Viviroli, D., & Weingartner, R. (2004). Mountains of the world: Vulnerable water towers for the 21st century. *Ambio*. Spec No 13:29-34. PMID: 15575180.

Milly, P. C. D., & Dunne, K. A. (2020). Colorado River flow dwindles as warming-driven loss of reflective snow energizes evaporation. *Science*, *367*(6483), 1252–1255. https://doi.org/10.1126/science.aay9187

Mizukami, N., Clark, M. P., Slater, A. G., Brekke, L. D., Elsner, M. M., Arnold, J. R., & Gangopadhyay, S. (2014). Hydrologic implications of different large-scale meteorological model forcing datasets in mountainous regions. *Journal of Hydrometeorology*, 474–488. https://doi.org/10.1175/JHM-D-13-036.1

Mote, P. W., Li, S., Lettenmaier, D. P., Xiao, M., & Engel, R. (2018). Dramatic declines in snowpack in the western US. *npj Climate and Atmospheric Science*, *1*, 2. https://doi.org/10.1038/s41612-018-0012-1

Ohmura, A. (2001). Physical basis for the temperature-based melt-index method. *Journal of Applied Meteorology and Climatology*, *40*, 753–761. https://doi.org/10.1175/1520-0450(2001)040<0753:PBFTTB>2.0.CO;2

Olyphant, G. A. (1986). Longwave radiation in mountainous areas and its influence on the energy balance of alpine snowfields. *Water Resources Research*, *22*(1), 62–66. https://doi.org/10.1029/WR022i001p00062

Painter, T. H., Berisford, D. F., Boardman, J. W., Bormann, K. J., Deems, J. S., Gehrke, F., et al. (2016). The Airborne Snow Observatory: Fusion of scanning lidar, imaging spectrometer, and physically-based modeling for mapping snow water equivalent and snow albedo. *Remote Sensing of Environment*, *184*, 139–152. https://doi.org/10.1016/j.rse.2016.06.018

Palazzi, E., Mortarini, L., & Terzago, S. (2019). Elevation-dependent warming in global climate model simulations at high spatial resolution. *Climate Dynamics*, *52*, 2685–2702. https://doi.org/10.1007/s00382-018-4287-z

Plüss, C., & Ohmura, A. (1997). Longwave radiation on snow-covered mountainous surfaces. *Journal of Applied Meteorology*, *36*, 818–824. https://journals.ametsoc.org/view/journals/apme/36/6/1520-0450-36.6.818.xml

Raleigh, M. S., Deems, J. S., & Collao-Barrios, G. C. (2019). Snowpack patterns in the east river, Colorado: Interannual consistency and relative hierarchy of contributing physical processes. In *AGU fall 2019 meeting*. Paper C33B-1573.

Raleigh, M. S., Lundquist, J. D., & Clark, M. P. (2015). Exploring the impact of forcing error characteristics on physically based snow simulations within a global sensitivity analysis framework. *Hydrology and Earth System Sciences*, *19*, 3153–3179. https://doi.org/10.5194/hess-19-3153-2015

Rhoades, A. M., Jones, A. D., & Ullrich, P. A. (2018). Assessing mountains as natural reservoirs with a multimetric framework. *Earth's Future*, *6*, 1221–1241. https://doi.org/10.1002/2017EF000789

Sicart, J. E., Pomeroy, J. W., Essery, R. L. H., & Bewley, D. (2006). Incoming longwave radiation to melting snow: Observations, sensitivity and estimation in northern environments. *Hydrological Processes*, *20*, 3697–3708. https://doi.org/10.1002/hyp.6383

Singh, P., & Kumar, N. (1996). Determination of snowmelt factor in the Himalayan region. *Hydrological Sciences Journal*, 301–310. https://doi.org/10.1080/02626669609491504

Smyth, M. (2018). *ECOSTRESS level-1B resampling and geolocation algorithm theoretical basis document*. Retrieved from https://ecostress.jpl.nasa.gov/downloads/atbd/ECOSTRESS_L1_ATBD_Geolocation_2018-03-08.pdf

Sturm, M., Goldstein, M. A., & Parr, C. (2017). Water and life from snow: A trillion dollar science question. *Water Resources Research*, *53*, 3534–3544. https://doi.org/10.1002/2017WR020840

Tillman, F. D. (2015). Documentation of input datasets for the soil-water balance groundwater recharge model of the Upper Colorado River Basin. U.S. Geological Survey Open-File Report 2015–1160 (p. 17). https://doi.org/10.3133/ofr20151160

Unsworth, M. H., & Monteith, J. L. (1975). Long-wave radiation at the ground I. Angular distribution of incoming radiation. *Quarterly Journal of the Royal Meteorological Society*, *101*, 13–24. https://doi.org/10.1002/qj.49710142703

Wainwright, H. M., Steefel, C., Trutner, S. D., Henderson, A. N., Nikolopoulos, E. I., Wilmer, C. F., & Enquist, B. J. (2020). Satellite-derived foresummer drought sensitivity of plant productivity in rocky mountain headwater catchments: Spatial heterogeneity and geological-geomorphological control. *Environmental Research Letters*, *15*(8), 084018. https://doi.org/10.1088/1748-9326/ab8fd0

Yan, G., Jiao, Z. H., Wang, T., & Mu, X. (2020). Modeling surface longwave radiation over high-relief terrain. *Remote Sensing of Environment*, *237*, 111556. https://doi.org/10.1016/j.rse.2019.111556

Yan, G., Wang, T., Jiao, Z., Mu, X., Zhao, J., & Chen, L. (2016). Topographic radiation modeling and spatial scaling of clear-sky land surface longwave radiation over rugged terrain. *Remote Sensing of Environment*, *172*, 15–27. https://doi.org/10.1016/j.rse.2015.10.026

Zakšek, K., Oštir, K., & Kokalj, Ž. (2011). Sky-view factor as a relief visualization technique. *Remote Sensing*, *3*, 398–415. https://doi.org/10.3390/rs3020398

Zhu, M., Yao, T., Yang, W., Xu, B., & Wang, X. (2017). Evaluation of parameterizations of incoming longwave radiation in the high-mountain region of the Tibetan plateau. *Journal of Applied Meteorology and Climatology*, 833–848. https://doi.org/10.1175/JAMC-D-16-0189.1

Zhu, X., Duan, S. B., Li, Z. L., Zhao, W., Wu, H., Leng, P., & Zhou, X. (2020). Retrieval of land surface temperature with topographic effect correction from Landsat 8 thermal infrared data in mountainous areas. *IEEE Transactions on Geoscience and Remote Sensing*, *59*(8), 6674–6687. https://doi.org/10.1109/TGRS.2020.3030900